LANGMUIR

pubs.acs.org/Langmuir Article

Benchmarking a Microfluidic-Based Filtration for Isolating Biological Particles

Fatih Inci*

Cite This: *Langmuir* 2022, 38, 1897−1909 Read Online

ACCESS | Metrics & More | Article Recommendations

ABSTRACT: Isolating particles from complex fluids is a crucial approach in multiple fields including biomedicine. In particular, biological matrices contain a myriad of distinct particles with different sizes and structures. Extracellular vesicles (EVs), for instance, are nanosized particles carrying vital information from donor to recipient cells, and they have garnered significant impact on disease diagnostics, drug delivery, and theranostics applications. Among all the EV types, exosome particles are one of the smallest entities, sizing from 30 to 100 nm. Separating such small substances from a complex media such as tissue culture and serum is still one of the most challenging steps in this field. Membrane filtration is one of the convenient approaches for these operations; yet clogging, low-recovery, and high fouling are still major obstacles. In this study, we design a two-filter-integrated microfluidic device focusing on dead-end and cross-flow processes at the same time, thereby minimizing any interfering factors on the recovery. The design of this platform is also numerically assessed to understand pressure-drop and flow rate effects over the procedure. As a model, we isolate exosome particles from human embryonic kidney cells cultured in different conditions, which also mimic complex fluids such as serum. Moreover, by altering the flow direction, we refresh the membranes for minimizing clogging issues and benchmark the platform performance for multitime use. By comprehensively analyzing the design and operation parameters of this platform, we address the aforementioned existing barriers in the recovery, clogging, and fouling factors, thereby achieving the use of a microfluidic device multiple times for bio-nanoparticle isolation without any notable issues.

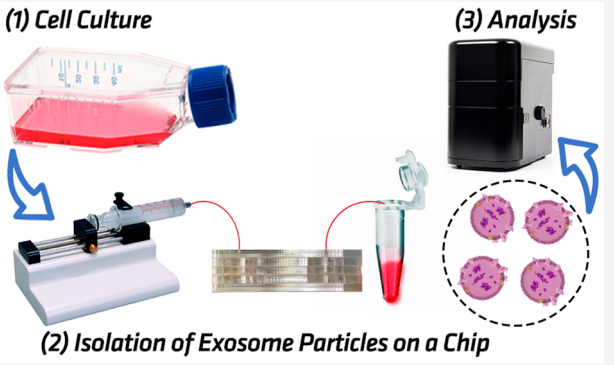

INTRODUCTION

The membrane is a barrier that enables the separation of particles in a mixture. The difference in the transport rate of each species through the membrane is the basic concept of membrane separation processes. Membranes are classified as two main groups of porous and nonporous characteristics. In porous membranes, the separation occurs due to the differences in size, shape, diffusion, and charge of species.[1] In the nonporous membrane case, the separation relies on the diffusion and selective adsorption.[2] Membrane separation processes can be classified into microfiltration, ultrafiltration, nanofiltration, and reverse osmosis considering particle size and the separation mechanism.[3] Among aforementioned methods, the ultrafiltration systems, in particular, are capable of separating particles with a size of 1−200 nm, which makes them useful for different biological particle separation, such as viruses, proteins, antibodies, vitamins, sugars, pyrogens, and extracellular vesicles.[4−11] For instance, extracellular vesicles (EVs) are one of the most crucial players in many cellular processes.[12] They are basically host cell-derived cargos, carrying molecular and genetic information in cell−cell communications and they allow cells to rid themselves of unwanted constituents.[13] Although EVs were initially defined as artifacts or cell dust,[14] there is growing evidence for their essential roles as messengers in physiological functions and for their contribution in the development and propagation of many diseases.[13,15−18] Recent evidence represents EVs as promising biological agents for both diagnostic and therapeutic approaches in personalized medicine and precision health.[19−21] Although there is still no consensus for the nomenclature of these cargos, EVs are basically classified based on their size, biogenesis, and biomarkers.[19,22,23] In principle, exosomes, the smallest EVs (30−100 nm in size), originate from the endosomal pathway, and they are secreted from intracellular multivesicular bodies (MVBs).[19,24,25] Microvesicles or microparticles, spanning from 100 to 1000 nm, are shed directly from the plasma membrane, and they are the product of exocytic budding,[16] whereas

Received: November 21, 2021
Revised: December 29, 2021
Published: January 18, 2022

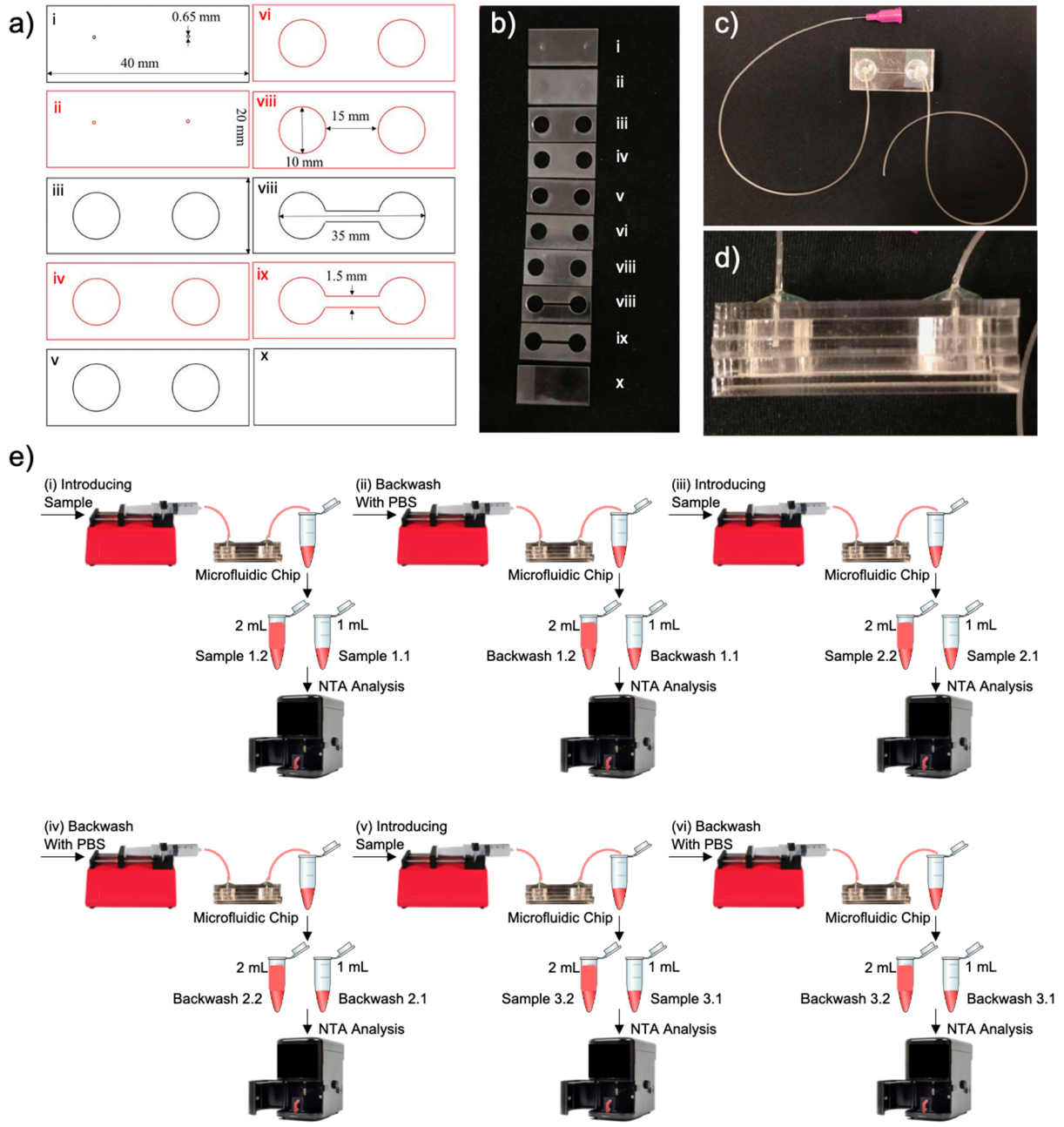

Figure 1. Microfluidic chip for the isolation of exosome particles. (a) Design parameters of the microfluidic chip is displayed. Roman numbers indicate the assembly order of the chip components from the top-layer to the bottom-layer. Numbers/drawings with black color state PMMA layers, whereas the numbers/drawings with red color represent DSA films. (b) Microfluidic chip consists of multilayers of PMMA and DSA films that integrate two filter membranes (200 and 50 nm of diameters). The assembly order of the chip contents is demonstrated. (c) Sampling and collecting the isolated particles are employed through tubings that are connected on inlet and outlet ports, respectively. (d) Side view of the chip is presented. (e) The schematic of sample and backwash processes is shown. Roman numbers state the process order in the work-flow. Briefly, (i) the sample solution is introduced into the microfluidic chip, and the particles are obtained in either 1 or 2 mL of the collected volume (sample 1.1 and 1.2). (ii) To refresh the filter membranes, the backwash step is employed by withdrawing either 1 or 2 mL of PBS solution through a syringe pump (backwash 1.1 and 1.2). These cycles are repeated with the (iii) sample (samples 2.1 and 2.2), (iv) backwash steps (backwash 2.1 and 2.2), (v) sample (samples 3.1 and 3.2), and finally (vi) backwash steps (backwash 3.1 and 3.2). At each step, either 1 or 2 mL of sample volume is collected as indicated in the schematic.

apoptotic bodies are the artifacts of cellular degradation during apoptosis.[13] For the collection of such nanosized particles, there are a variety of isolation techniques, including differential centrifugation, ultracentrifugation, size-exclusion chromatography, precipitation-based methods, immunoaffinity, and ultrafiltration.[26,27] Among these methods, the ultrafiltration isolates particles based on the difference in their size.[28,29] Briefly, there are typically two types of strategies, including dead-end and cross-flow (tangential-flow). In the dead-end process, all sample is perpendicularly introduced to the surface of the membrane, resulting in the accumulation of the rejected particles across the surface of the membrane. After a while, the thickness of the rejected particles layer increases and not only does the pressure drop increase but also the quality of the permeate decreases. On the other hand, in cross-flow operations, the sample passes along with the membrane surface, and hence the clogging is lower

https://doi.org/10.1021/acs.langmuir.1c03119
Langmuir 2022, 38, 1897−1909

compared to the dead-end membrane configuration. Compared with the cross-flow, the main advantage of the dead-end method is its high recovery.

Here, we demonstrate a hybrid approach that combines both dead-end and cross-flow processes on a single microfluidic chip, thereby benefiting from the advantage of both techniques that potentially results in a high recovery and lower clogging tendency. As a model application, we here isolate exosome particles from human embryonic kidney cells (HEK293), and at the same time, we comprehensively benchmark the platform with a variety of biological conditions while culturing the cells in order to evaluate any effects in the isolation of particles. Moreover, we assess this filtration process and potential pressure drop through numerical assessments and simulations. In our design, the microfluidic chip consists of two different filter membranes, and the sample is basically injected through the first membrane (200 nm of pore diameter) as a dead-end filtration strategy. This membrane eliminates large debris in biological matrices, and through the microfluidic channel, the first filtrate reaches the second membrane (50 nm of pore diameter) to isolate the particles through a cross-flow strategy. In order to refresh the membrane for minimizing any possible cake formations, we also introduce physiological buffer to the membranes to back-flush the filters, hence altering the flow directions and the filtration strategies on the chip. In addition to high recovery and lower fouling manners, we have achieved the employment of this platform multiple times without any significant reductions in the operation performance.

EXPERIMENTAL SECTION

Materials. To fabricate microfluidic chips, poly(methyl methacrylate) (PMMA) was purchased from Sumitomo Chemical (Singapore), double-sided adhesive (DSA) films were obtained from 3M (Saint Paul, MI, United States), Tygon-brand of tubings was purchased from Cole Palmer (Vernon Hills, IL, United States), and Whatman Nuclepore Track-Etched Membranes (200 and 50 nm) were obtained from MilliporeSigma (Burlington, MA, United States). The HEK293 cells (ATCC CRL-1573 HEK293) were purchased from ATCC (Manassas, VA, United States), which is a nonprofit, global biological resource center and standards organization as the supplier of authenticated cell lines worldwide. The HEK293 cell line has been widely used in cell biology and biotechnology.[30] By closely following the procedure from the literature,[31] we only cultured these cells, and only collected extracellular particles from their supernatants. After isolating exosome particles on-chip, we only measured their sizes, concentration, and size distribution, and then, these particles were discarded immediately. In this study, we did not collect any genomic information from these cells, and also, we did not perform any transformation experiments with these cells. Dulbecco's Modified Eagle Medium/Nutrient Mixture F-12 (DMEM/F-12) and 10% of Fetal Bovine Serum (FBS) were obtained from Biowest (Nuaillé, France). Penicillin/Streptomycin (1% and 5 mL) and 1% of L-glutamine were purchased from Gibco-Thermo Fisher Scientific (Waltham, MA, United States).

Fabrication of Microfluidic Chip. The components of the microfluidic device consisted of PMMA (2 mm of thickness), DSA film (50 μm of thickness), and two filters (200 and 50 nm of pore sizes). The PMMA layers formed the appropriate surfaces to introduce and collect samples, whereas the DSA film enabled one to assemble the PMMA layers and filters, as well as allowed for the formation of a microfluidic channel. As depicted in Figure 1a,b, the layers of (i) and (ii) indicated the first PMMA layer (20 × 40 mm) and DSA film to create the inlet and outlet ports; the layers of (iii)−(vii) were designated to create a reservoir for the sample filtration, and the filter membranes (200 and 50 nm) were integrated after the layer of (vii); the layers of (viii) and (ix) generated a microfluidic channel to transfer the filtrated samples to the outlet port; and the layer of (x) was placed at the bottom of the channel for the flow. All these design and fabrication processes were performed using RDWorks V8 software and LazerFix (Turkey) instrument, respectively. The final format of the microfluidic chip was achieved by simply adhering all these components by using DSA films (Figure 1c,d). In this design, sampling was applied through the inlet port, and exosome particles were collected from the outlet port. All the sampling and collection ports were integrated with tubings for a facile process.

Cell Culture. HEK293 cells were used as a model resource for the production of exosome particles in order to benchmark the performance of the microfluidic chip. In accordance with the literature,[31] cells were grown in DMEM/F-12 (500 mL), and penicillin/streptomycin (1% and 5 mL), 1% of L-glutamine (5 mL), and 10% of FBS (50 mL) were added into the medium as supplements.

Sample Preparation. Here, we designed three sets of experiments to benchmark the chip with high complex solutions. We defined the group (i) while using FBS solution itself as a source of exosome particles since the FBS solution includes extracellular vesicles including exosomes potentially.[32,33] To prepare samples for the particle isolation from cell culture samples, the medium was collected from each condition (cells cultured in FBS-containing medium: the group (ii), and FBS-free medium: the group (iii)) separately on the fourth day of culture after the medium was changed. Following this step, the medium was added into a falcon tube and centrifuged at 20,000 g (14,000 rpm) for 5 min at room temperature, thereby precipitating very large particles and cell debris before applying the medium into the chip. After the centrifugation, since the supernatant contains exosome particles, this part was transferred to a new tube and used in the experiments. Finally, to avoid bacterial or other contaminations, the supernatant was passed through a 0.22 μm syringe filter, and it was then ready for the microfluidic chip experiments. The same steps were carried out for FBS solution as a control (the group (i)).

Exosome Particle Isolation. To understand the content of supernatant described above, we initially run the Nanosight Nanoparticle Tracking Analysis (NTA) (NS300, Malvern Instruments Ltd., Malvern, Worcestershire, UK) for "stock sample", in which the supernatant was passed through a 0.22 μm syringe filter, and it was not applied into a microfluidic chip. In the microfluidic chip experiments, we conducted two different experimental sets by changing the collected volumes of "sample" (either 1 or 2 mL). The inlet of the device was connected to the syringe tip, and the outlet was placed in 2 mL Eppendorf tubes. The inlet flow rate was set as 40 μL/min. Similarly, in order to refresh the filter surface from any potential cake formations, we also performed a "backwash" step by withdrawing either 1 or 2 mL of PBS solution through a syringe pump with 60 μL/min of flow rate. "Sample" and "backwash" steps were sequentially repeated three times to demonstrate the reusability of this platform. All these steps were applied for group (i) as well. For convenience, we demonstrated the nomenclature of all "sample" and "backwash" steps in Figure 1e.

Particle Characterization Assays. To analyze the concentration, diameter and size distributions of exosome particles, we employed NTA instrument, which employs a laser-based optical technique that monitors Brownian motion of singular particles in solution. The system is coupled with an embedded 488 nm laser (blue) instrument since the diameter of the particles is within in the range of optical features of this laser. After introducing the sample into the instrument, the diameter of particles was determined using the Stokes−Einstein equation, and the size distribution and number of particles were measured and quantified accordingly. In the analysis, distilled water was first passed 4−5 times through the NTA Instruments to calibrate the system and remove any potential artifacts before the measurements. Once the cleaning process was done, the values such as viscosity, temperature, and dilution rates were set before the measurements. For each sample, five video recordings with 60 s duration each were applied.

Scanning Electron Microscope. The isolated exosome particles were characterized via a scanning electron microscope (SEM). Briefly, a silicon wafer was employed as a base material for the imaging. The wafer was first cleaned via three sonication steps for 5 min intervals with acetone, ethanol, and water, respectively. The collected samples were mixed (1:1, v:v) with 2% paraformaldehyde, thereby fixing the particles

https://doi.org/10.1021/acs.langmuir.1c03119
Langmuir 2022, 38, 1897−1909

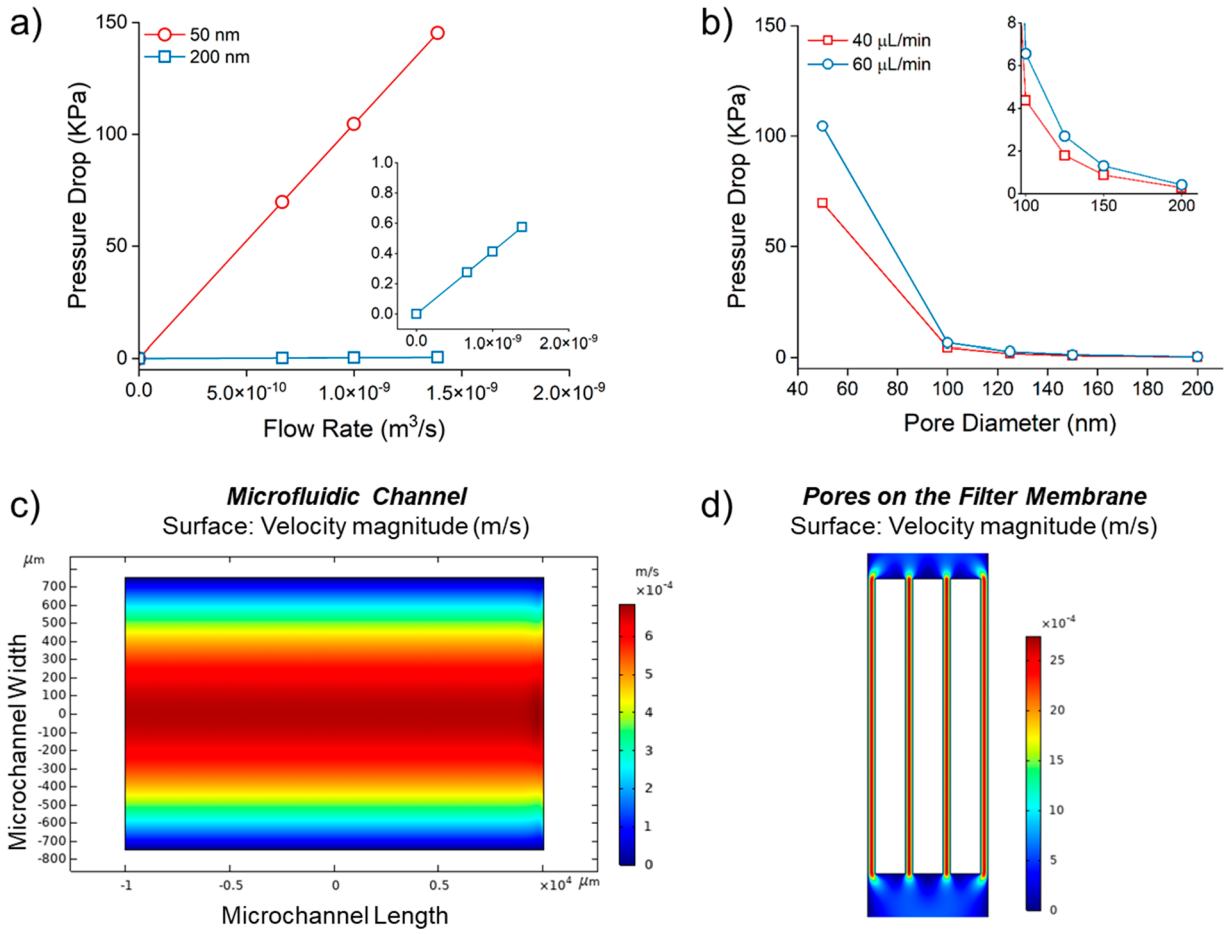

Figure 2. Numerical simulations. (a) The pressure drop versus flow rate while changing the pore diameters of the filter membrane. (b) Pressure drop versus filter pore diameters on the course of various flow rates applied during the process. (c) While applying a flow rate of 40 μL/min, the simulation of velocity field in the microchannel and (d) across the membrane pores is presented.

to keep their intact structure as much as possible. Before the imaging, 5 nm of gold/palladium coating was applied to the wafer surface.

Statistical Analysis. To assess the performance and the yield capacity of the chips, we analyzed all the data statistically using Violin-shaped Box–Whisker plots and further evaluated through non-parametric Kruskal–Wallis analysis followed by Dunn's multiple comparison test.

RESULTS AND DISCUSSION

Numerical Modeling for Membrane Filtration. In our approach, we first studied the impact of various parameters on the fluid flow across the membrane. In this way, u is the average velocity of the fluid inside the pore, ρ is density of the fluid, t is the pore thickness (also the pore length), a is the pore radius, μ is the dynamic viscosity of the fluid, and Δp is the pressure difference across the membrane. In consideration of the previous studies carried out by Sampson,[34] Weissberg,[35] and Dagan,[36] we here aimed to find the appropriate approach in order to define the relationship between various parameters, affecting the flow rate across the membrane. Briefly, Sampson solved the Navier–Stokes equations, assuming that the inertial forces were ignored for an incompressible flow passing through a circular pore in an infinite plate. Considering the above assumptions, continuity and Naiver-Stokes equations were shown in eq 1.

$$\nabla \cdot u = 0, \quad \mu \nabla^2 u - \nabla p = 0 \tag{1}$$

Sampson considered the following relation between the flow rate and the pressure difference by resolving the above equations. As a note, the following equation is valid for the infinite thin plate (eq 2). For several applications, where the pore thickness (t) is comparable to the pore radius (a), an additional resistant and therefore pressure drop is applied to the fluid due to the plate thickness. Poiseuille flow into the pore is considered to find the pressure drop related to the thickness effect (eq 3). Since the resistance proposed by Sampson and Poiseuille are in series, they can be superimposed. The following equation is true for Re $\ll$ 1 and that for different values of thickness and pore radius, the error of linearly adding two terms is less than 1%.

$$\frac{\Delta p}{q} = \frac{3\mu}{a^3} \tag{2}$$

$$\frac{\Delta p}{q} = \frac{8\mu t}{\pi a^4} \tag{3}$$

The superimposed equation is defined in eq 4.[36] The model provides that in each membrane, there are specified numbers of pores in parallel, and the pressure across each pore is equal to the total pressure drop while the total flow rate (Q) is equal to the summation of the flow in each pore (q). Therefore, the eq 4 is described as follows for the total number of pores in the membrane (N), as defined in eq 5.

https://doi.org/10.1021/acs.langmuir.1c03119
Langmuir 2022, 38, 1897−1909

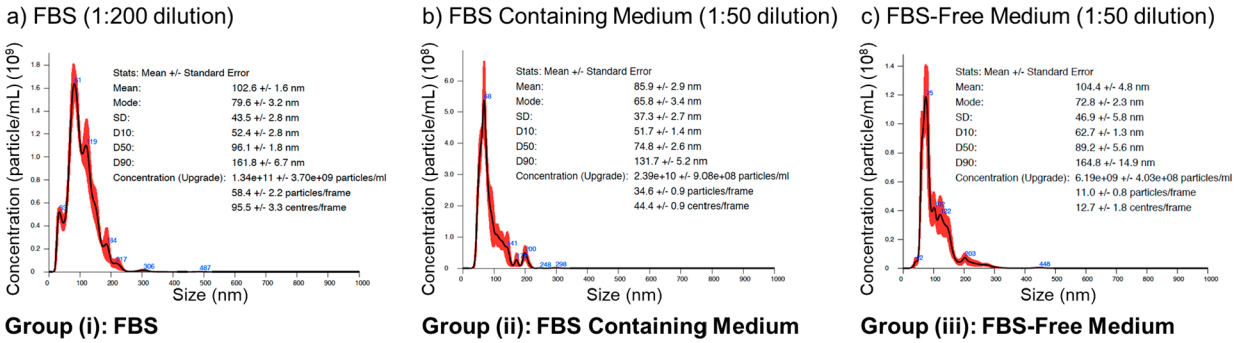

Figure 3. NTA analysis of stock samples. The particle analysis for (a) group (i), (b) group (ii), and (c) group (iii). This analysis provides information on the concentration, size, and size distribution of the isolated particles.

$$\frac{\Delta p}{q} = \frac{3\mu}{a^3} + \frac{8\mu t}{\pi a^4} \tag{4}$$

$$\frac{\Delta p}{Q/N} = \frac{3\mu}{a^3} + \frac{8\mu t}{\pi a^4} \tag{5}$$

With regard to our polycarbonate track-etched membranes used in our design, the following data were obtained, and it would be used for the further analysis:

$$N = 6 \times 10^8,\ a = 25\ \text{nm (the diameter of a pore} = 50\ \text{nm}),\ t = 8\ \mu\text{m},\ \mu = 1.2\ \text{mPa·S}$$

For the flow rate of 40 μL/min (0.666×10^{-9} m^3/s), the pressure drop on the membrane having the pores with 50 nm of diameter was calculated as follows:

$$\Delta p = \frac{0.666 \times 10^{-9}}{6 \times 10^8} \times \left(\frac{3 \times 0.0012}{(0.000000025)^3} + \frac{8 \times 0.0012 \times 0.000008}{\pi \times (0.000000025)^4} \right) = 69.757\ \text{kPa}$$

Similarly, the pressure drop for 200 nm of diameter is 0.276 kPa. By the use of eq 5, the pressure drop values on different filter membranes with 50 and 200 nm versus various flow rates were plotted (Figure 2a). Upper limit of the flow rate and pressure drop could be determined by using a different pump with stronger motor power. In order to find the relation between pressure drop and the pore size, two constant flow rates were considered since 40 μL/min and 60 μL/min (0.999×10^{-9} m^3/s) were applied in "sample" and "backwash" steps (Figure 2b). While changing the flow rate to 60 μL/min for the backwash steps, the pressure drop values were calculated as 104.636 kPa and 0.413 kPa for 50 and 200 nm of the filters, respectively. Here, we concluded that as the membrane pore size increases, the pressure drop across the membrane decreases, and it is therefore possible to increase the flow rate. Moreover, increasing the flow rate in the backwash steps was sufficient due to the flow direction. In consideration of the reported diameters of exosome particles (30−100 nm in size),[19,24] increasing the membrane pore size would interfere with the recovery efficiency since larger particles would pass through the membrane. Therefore, we applied varying flow rates onto the membranes with the fixed pore sizes.

Numerical Simulations for Fluid Flow. The system of interest in this study was to create the fluid flow in the two-dimensional (2D) flow over two membranes embedded in the microchannels. The inlet flow rate of the fluid was considered as 40 μL/min while introducing the "sample" into the channel for isolating exosome particles. In the case of "backwash", the flow rate of the withdrawn fluid was stated as 60 μL/min. In addition to the membrane characteristics stated above, the flow was laminar, steady, viscous, and incompressible in this fluid flow simulation. As we described the order of chip layers above, the fluid flows through the inlet and reaches the reservoir formed by the PMMA layers, and then, it penetrates into the first membrane with a thickness of 8 μm and pore size of 200 nm. After crossing the filter, the fluid travels through the microchannel with the length of 35 mm and width of the 1.5 mm. Once the fluid reaches to the end of the microchannel, it repeats the same path as its inlet and passes to go to the outlet. In this way, it penetrates into the second membrane with the pore size of 50 nm and passes through to exit from the hole on the first PMMA layer. In accordance with this path, the computational domain was presented (i) while the fluid travels into the microchannel (Figure 2c) and also (ii) while passing the filter membrane (Figure 2d). In the simulations, the grids were refined near the microchannel walls. A grid independence test was carried out to guaranty that the results were independent of the number of grids. This test was performed for three grid numbers at different inlet and outlet velocities at the center of the microchannel, and the grid number of 15,248 was selected for all the calculations.

To understand velocity profile across the microchannel and membranes, we simulated velocity magnitude into the microchannel as presented in Figure 2c. Considering that the fluid flow in the microchannel was laminar, and the Reynolds number was low ($Re \sim 1$), the velocity profile showed that the maximum velocity occurred in the middle of the channel, and the fluid velocity was zero at the boundary surfaces due to the no-slip boundary condition. In Figure 2d, the velocity profile of the fluid across the membrane was illustrated. The figure exhibited a membrane with the thickness of 8 μm and pore size of 200 nm. In consideration of the computing power for the simulation, we here demonstrated only four pores in the membrane. The fluid starts from the top and when it reached to the surface of the membrane, the fluid was able to only penetrate through the pores with specified pore size and thickness. According to the continuity equation, the cross section of the fluid path decreased while it reached to the membrane, and also, the fluid velocity increased and the velocity was higher into the pores compared with its velocity before entering the pores.

https://doi.org/10.1021/acs.langmuir.1c03119
Langmuir 2022, 38, 1897−1909

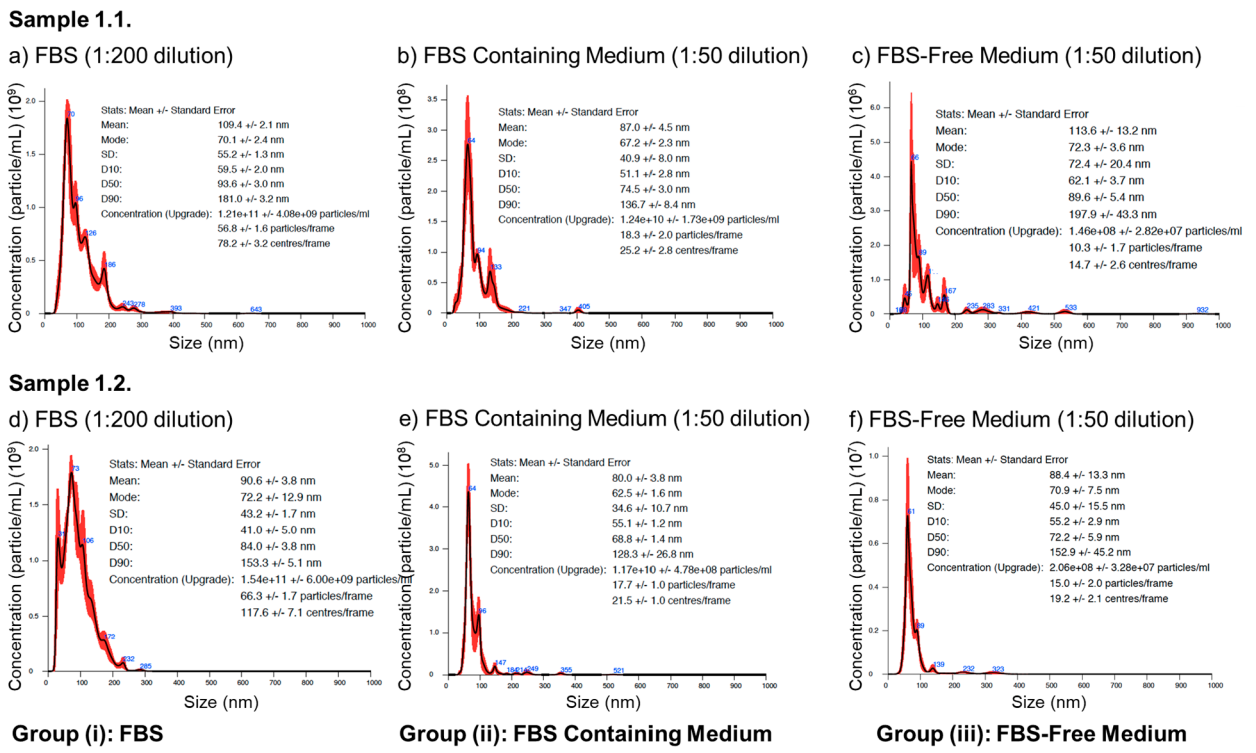

Figure 4. NTA analysis of samples. The particle analysis is performed for different groups and various volumes. Sample 1.1 indicates that 1 mL of sample is introduced into the microfluidic chip, and the particle analysis is applied for (a) group (i), (b) group (ii), and (c) group (iii). Likewise, sample 1.2 states that 2 mL of sample is applied into the microfluidic chip, and the particle analysis is applied for (d) group (i), (e) group (ii), and (f) group (iii). This analysis provides information on the concentration, size, and size distribution of the isolated particles.

Particle Isolation on a Microfluidic Chip. As aforementioned, we designed a microfluidic chip employing both dead-end and cross-flow (tangential-flow) through two separate filter membranes with different directions of flow, thereby separating exosome particles through a step-by-step serial filtration, as well as eliminating undesired components based on the size. As described earlier, we evaluated three different experimental sets: group (i) indicates FBS sample without any cellular contents (control); group (ii) states supernatant collected from cells grown in the medium containing FBS; and group (iii) represents supernatant collected from cells grown in FBS-free medium. All these samples were named as "stock samples", which were not introduced to the microfluidic chip, but they were only filtered through 0.22 μm filter before the NTA measurements. Initially, the NTA analysis was carried out to determine the concentrations, diameter, and size distributions of particles collected from stock samples. Here, we observed different particles with various concentrations, means, and mode values (Figure 3). For instance, group (i) provided $1.34 \times 10^{11} \pm 3.7 \times 10^{9}$ particles/mL of the particle concentration along with 102.6 $\pm$ 1.6 nm and 79.6 $\pm$ 3.2 nm of mean and mode values, respectively (Figure 3a). Group (i) also provided larger fluctuations in particle size distributions compared to the other groups. Group (ii) provided $2.39 \times 10^{10} \pm 9.08 \times 10^{8}$ particles/mL of concentration along with 85.9 $\pm$ 2.9 nm and 65.8 $\pm$ 3.4 nm of mean and mode values, respectively (Figure 3b). On the other hand, the particles collected from group (iii) resulted in $6.19 \times 10^{9} \pm 4.03 \times 10^{8}$ particles/mL of concentration along with 104.4 $\pm$ 4.8 nm and 72.8 $\pm$ 2.3 nm of mean and mode values, respectively (Figure 3c). Both the groups (ii) and (iii) provided more narrow size distributions, having higher tendency to be monodisperse particles, yet containing a lower number of particles compared to the group (i).

In the microfluidic experiments, we applied the samples through a syringe pump system. To analyze the effect of the collected volume, we filtered 1 mL (sample 1.1) and 2 mL (sample 1.2) of supernatant through the chip. To refresh the surface of filter membranes, the syringe pump withdrew (only changing the flow direction) around 1 and 2 mL of PBS, thereby removing the particles, which were not able to pass to the filtrate solution due to their sizes and/or any potential cake formations. These collected samples were tagged as "backwash 1.1" for 1 mL of collection and "backwash 1.2" for 2 mL of collection. After each sample was collected, the dilutions were prepared and analyzed through the NTA. As a note, due to a high number of particles in group (i), we particularly diluted this sample as either 1:100 or 1:200 to obtain more accurate results, whereas the samples from the groups (ii) and (iii) were diluted less or undiluted due to the low number of particles. All these dilution rates were indicated on the plots, and they were considered during the calculation of particle concentrations. Per the NTA results for sample 1.1 solutions, the group (i) provided $1.21 \times 10^{11} \pm 4.08 \times 10^{9}$ particles/mL, along with 109.4 $\pm$ 2.1 nm and 70.1 $\pm$ 2.4 nm of mean and mode values, respectively (Figure 4a). In consideration of the results derived from the stock sample of group (i) (Figure 3a), the filtration through a microfluidic chip altered the size distribution of particles in group (i). On the other hand, the particles collected from group (ii) resulted in $1.24 \times 10^{10} \pm 1.73 \times 10^{9}$ particles/mL, and their mean and mode values were 87.0 $\pm$ 4.5 nm and 67.2 $\pm$ 2.3 nm, respectively (Figure 4b) that were more monodisperse particles with around half concentration of the particles in Figure 3b. Moreover, the particles collected from group (iii) resulted in

https://doi.org/10.1021/acs.langmuir.1c03119
Langmuir 2022, 38, 1897−1909

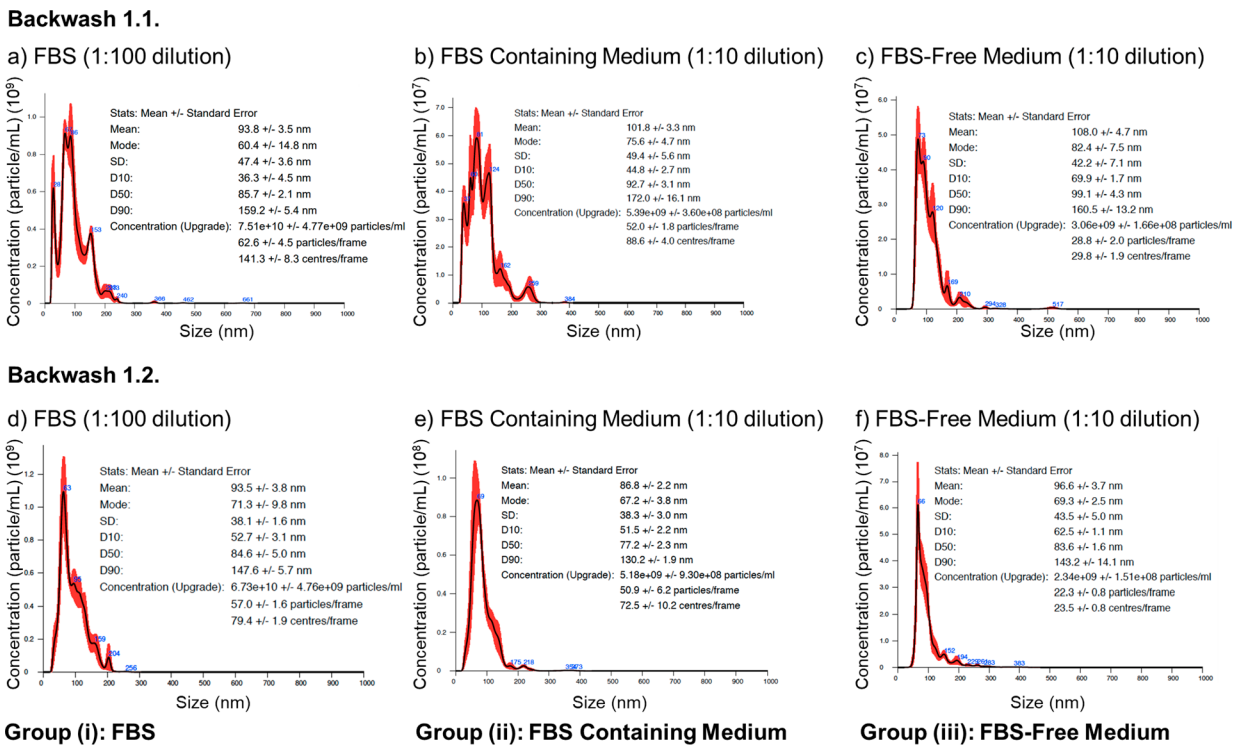

Figure 5. NTA analysis of backwash. The particle analysis is performed for various groups and different volumes. Backwash 1.1 states that 1 mL of sample is collected from the microfluidic chip after a backwash step, and the particle analysis is employed for (a) group (i), (b) group (ii), and (c) group (iii). Similarly, backwash 1.2 indicates that 2 mL of sample is collected from the microfluidic chip after a backwash step, and the particle analysis is performed for (d) group (i), (e) group (ii), and (f) group (iii). This analysis shows information on the concentration, size, and size distribution of the isolated particles.

$1.46 \times 10^8 \pm 2.82 \times 10^7$ particles/mL of concentration along with 113.6 ± 13.2 nm and 72.3 ± 3.6 nm of mean and mode values, respectively (Figure 4c). Compared with the results between Figures 3c and 4c, we observed a sharper peak around the mean value, yet the concentration reduced >40 times. Consequently, while comparing all the results of sample 1.1 with their stock samples individually, we clearly achieved the filtration process, leading to a reduction in the particle concentrations, as well as generating more monodispersity around the mean values of particles (Figures 3 and 4). With consideration of all sample 1.1 data internally (Figure 4a–c), group (i) resulted in higher concentrations of particles than those of the other conditions, whereas the particles collected from the groups (ii) and (iii) provided more narrow size-distributions, noting that more monodisperse particles.

In sample 1.2 solutions, increasing the collected volume enabled higher tendency to a monodispersity for each group (except group (i)), pointing out that 1 mL of filtrate collection was not enough in the current design for filtering properly. Briefly, group (i) provided $1.54 \times 10^{11} \pm 6.0 \times 10^9$ particles/mL, and the mean and mode values were 90.6 ± 3.8 nm and 72.2 ± 12.9 nm, respectively (Figure 4d). Comparing these results with Figure 4a, the concentration of particles increased relatively due to the collection of larger volume, and also, the particle diameter decreased since larger volume provided a broader range of particles with different sizes. In group (ii), sample 1.2 provided $1.17 \times 10^{10} \pm 4.78 \times 10^8$ particles/mL, containing the particles with 80.0 ± 3.8 nm of mean and 62.5 ± 1.6 nm of mode values (Figure 4e). On the other hand, sample 1.2 of group (iii) resulted in $2.06 \times 10^8 \pm 3.28 \times 10^7$ particles/mL, and the mean and mode values were calculated as 88.4 ± 13.3 nm and 70.9 ± 7.5 nm, respectively (Figure 4f). Consequently, in all groups, we observed a decrease in the particle size.

In backwash 1.1 experiments, group (i) resulted in $7.51 \times 10^{10} \pm 4.77 \times 10^9$ particles/mL, containing the particles with 93.8 ± 3.5 nm and 60.4 ± 14.8 nm of mean and mode values, respectively (Figure 5a). While comparing these data with Figure 4a, we collected a lower number of particles, stating more particles had already passed through the filter, yet the particle dispersity was higher. When considering the decrease in the diameter of collected particles from ∼109.4 nm to ∼93.8, there might be a cake formation on the filter membrane facing toward the microchannel. The particles collected from group (ii) were counted as $5.39 \times 10^9 \pm 3.60 \times 10^8$ particles/mL, and they had 101.8 ± 3.3 nm of mean and 75.6 ± 4.7 nm of mode values (Figure 5b). The particle numbers were >2 times lower than that of Figure 4b, and similarly, they were more polydisperse. On the other hand, group (iii) resulted in collecting $3.06 \times 10^9 \pm 1.66 \times 10^8$ particles/mL, including the particles with 108.0 ± 4.7 nm and 82.4 ± 7.5 nm of mean and mode values, respectively (Figure 5c). In the case of group (iii), the concentration of particles collected from backwash 1.1 was ∼20 times higher than of sample 1.1 of group (iii) (Figure 4c), pointing out that more particles might have been either stuck on the internal side of the filter membrane or they might have located in the channel. In consideration of all the data derived from backwash 1.1 and their counterparts in sample 1.1, we observed highly disperse particles with large fluctuations in their size distributions.

Evaluating the backwash 1.2 solutions, we similarly realized that higher volume was able to collect particles with more monodisperse characteristics, and it indicated again that volume was one of the critical parameters for the filtration process on the

https://doi.org/10.1021/acs.langmuir.1c03119
Langmuir 2022, 38, 1897−1909

chip. For instance, group (i) resulted in isolating $6.73 \times 10^{10} \pm 4.76 \times 10^{9}$ particles/mL, and their mean and mode values were 93.5 ± 3.8 nm and 71.3 ± 9.8 nm, respectively (Figure 5d). In group (ii), backwash 1.2 provided $5.18 \times 10^{9} \pm 9.3 \times 10^{8}$ particles/mL of concentration, along with 86.8 ± 2.2 nm of mean and 67.2 ± 3.8 nm of mode values (Figure 5e). On the other hand, backwash 1.2 of the group (iii) resulted in $2.34 \times 10^{9} \pm 1.51 \times 10^{8}$ particles/mL, including particles with 96.6 ± 3.7 nm and 69.3 ± 2.5 nm of mean and mode values, respectively (Figure 5f). In the backwashing experiments, increasing the collection volume from 1 to 2 mL did not alter the concentration of particles notably, and this stated that the required volume for backwashing would be either 1 mL or the volume between 1 and 2 mL. Considering lower volume needs and higher flow rates, the time required for the backwashing step would be further minimized. On the other hand, more volume enabled us to collect more monodisperse particles in all backwash cases, suggesting that higher volume improved the dispersity of the collected particles (Figure 5).

In addition, we benchmarked the performance of microfluidic chips for isolating the particles while using them multiple times sequentially in order to improve the yield and repeatability of the chip. In this manner, the chips were employed three times for "sample" processes to isolate the particles, and also, three "backwash" processes to refresh the surface of filter membranes after each sample process. As the first sample and backwash step was mentioned above, we continued with the second and third runs with these chips. Briefly, we observed a statistical difference between groups (i) and (iii) in all samples ($n = 5$, $p < 0.01$) (Figure 6). Furthermore, there was no significant difference between groups (i) and (ii) and between groups (ii) and (iii) ($n = 5$, $p > 00.5$). Since group (i) contains exosome particles intrinsically, group (i) provided the highest number of particles. The number of particles collected from group (ii) were lower than that of group (i), but it was not statistically meaningful ($n = 5$, $p > 0.05$). Basically, FBS provides three advantages to cells: (i) providing a supplement for *in vitro* cell culture; (ii) enabling cell adherence to the flask; and (iii) generating a unique biological makeup that promotes rapid cell growth and proliferation due to the abundance of growth factors.[37] Compared to group (i), a lower number of particles collected from group (ii) might be due to high utilization of the FBS during cell growth and adherence. On the other hand, the lowest number of particles was observed in group (iii), and this yield was ∼30 times lower than that of group (ii), yet it was not statistically different ($n = 5$, $p > 0.05$). This also pointed out that exosome particle yield was not notably affected by the FBS ingredient of *in vitro* culture of HEK293 cells. Moreover, the presented chip design was capable of processing in both FBS-containing and FBS-free medium. In this study, we only focused on the production yield of particles on both cases by employing a microfluidic chip; however, there might be some molecular effects in the production levels of particles while culturing cells either in the presence or absence of FBS in the medium, and this would be further analyzed through genomic or transcriptomic analyses.[38]

Second, we have focused on refreshing the filter surface through "backwash" processes (Figure 7). Likewise, in all "backwash" experiments, group (i) provided a greater number of particles compared to group (iii) ($n = 5$, $p < 0.01$). Only in backwash 2.2, we observed a difference of more than 95%, but less than 99% ($n = 5$, $p < 0.05$). Similarly, group (i) was also statistically different than group (ii) ($n = 5$, $p < 0.05$). While checking the number of particles collected in all cases at different backwash processes, group (i) had the lowest number of particles in backwash 2.2, pointing out this reduction in statistical significance, and this might be caused by any potential handling issues or any problems in the exosome particle isolation during this backwash process only. Similarly, the microfluidic

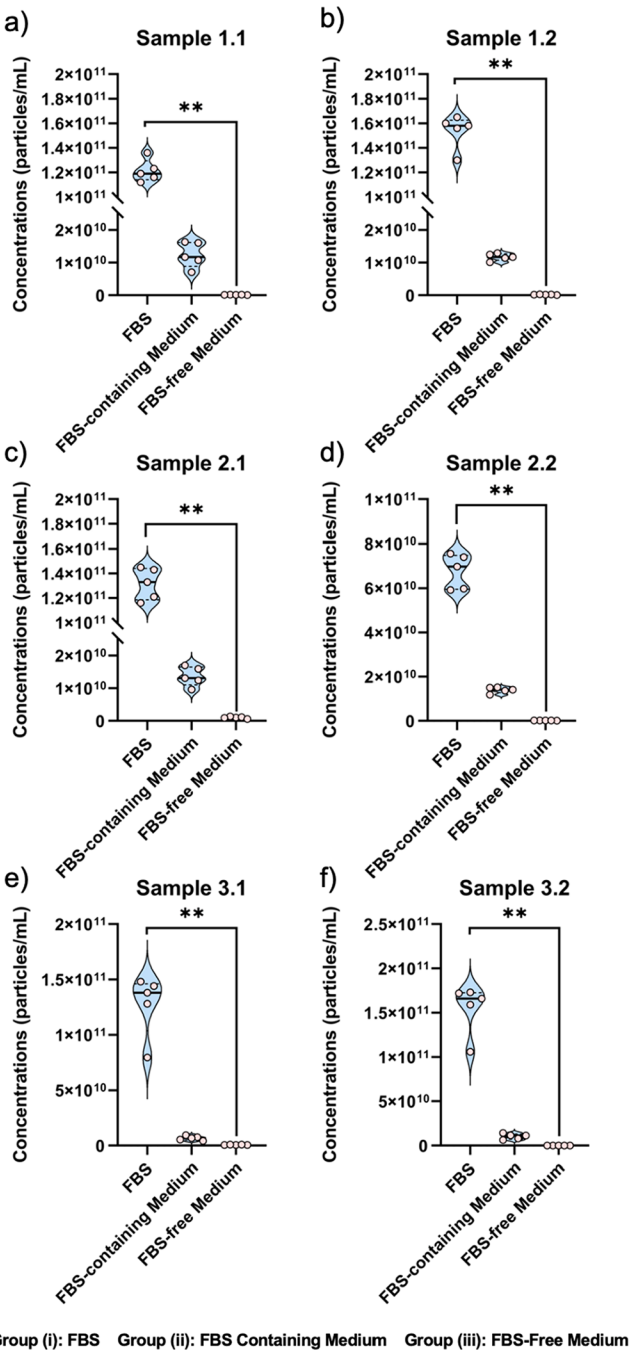

Figure 6. Assessing multiple use of microfluidic chips in terms of the particle yields of sample steps. In this experiment, different groups (i)−(iii) are compared in each run on the chip. The first run indicates sample 1, along with (a) 1 mL and (b) 2 mL of particle volumes. The second run states sample 2, and presents (c) 1 mL and (d) 2 mL of particle volumes. The third run demonstrates sample 3, along with (e) 1 mL and (f) 2 mL of particle volumes. Statistical assessments are performed using Violin-shaped Box−Whisker plots, and the data is further evaluated through nonparametric Kruskal−Wallis analysis followed by Dunn's multiple comparison test ($n = 5$; **: $p < 0.01$).

https://doi.org/10.1021/acs.langmuir.1c03119
Langmuir 2022, 38, 1897−1909

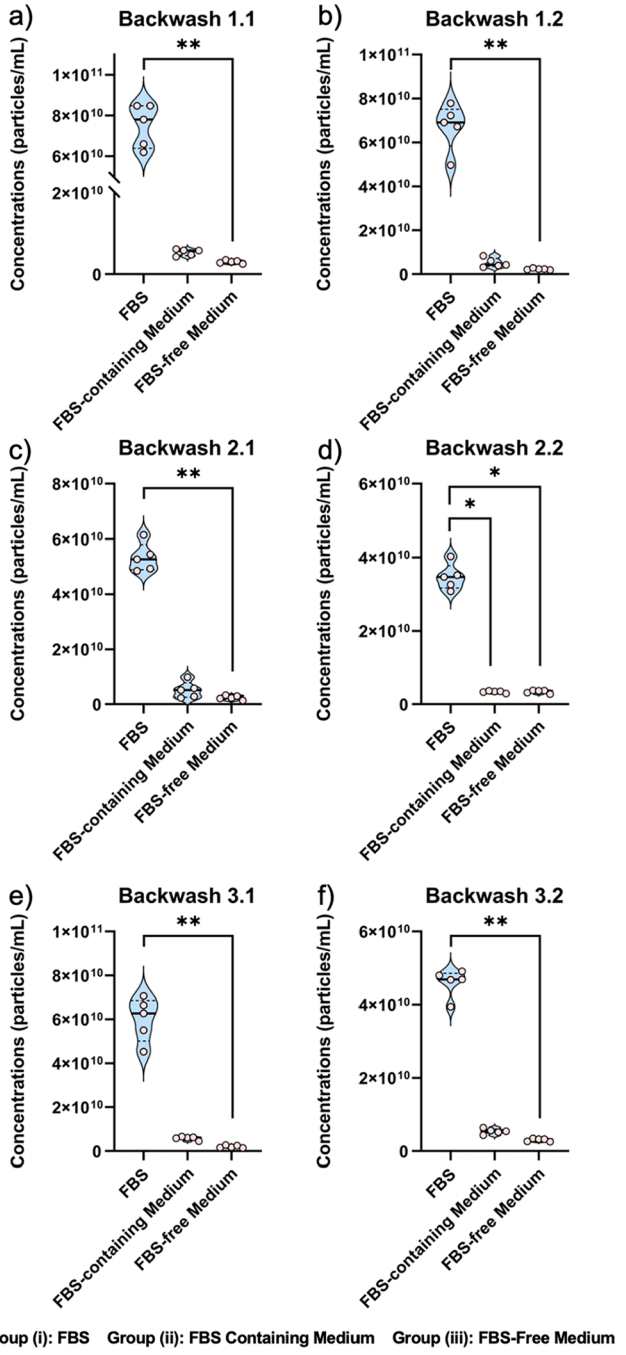

Figure 7. Evaluating multiple use of microfluidic chips in terms of the particle yields of backwash steps. Here, different groups (i)−(iii) are compared in each run on the chip. The first run states backwash 1, along with (a) 1 mL and (b) 2 mL of backwash volumes. The second run states backwash 2, and presents (c) 1 mL and (d) 2 mL of backwash volumes. The third run shows backwash 3, along with (e) 1 mL and (f) 2 mL of backwash volumes. Statistical assessments are performed using Violin-shaped Box−Whisker plots, and the data is further assessed through nonparametric Kruskal−Wallis analysis followed by Dunn's multiple comparison test ($n = 5$; *: $p < 0.05$; **: $p < 0.01$).

chip was able to recover the particles on the filter membranes and refresh the membrane for the next sample processes.

In addition, for three sample and three backwash runs, we evaluated the effect of the collected volume (1 or 2 mL) while isolating exosome particles (Figure 8). Since each sample had a unique feature, we compared only volume parameters in different groups. In group (i), we have observed a similar number of particles, indicating that the particle yield was independent from the volume parameter in group (i) samples ($n = 5$, $p > 0.05$) (Figure 8a). Although it was not statistically different, there were some fluctuations in the sample volumes. For instance, sample 2.1 provided ∼2 times higher yield compared to sample 2.2, having higher volume. Although higher volumes would be expected to produce more particles, we concluded that there were some collecting issues since serum proteins provided more condensed milieu, which might have interfered with the isolation of particles; or there might be some handling issues in higher volumes, yet it was only in sample 2 of the group (i). On the other hand, group (ii) provided ∼10 times lower yield compared to group (i) samples (Figures 8a,b). According to the statistical assessments, we did not observe any significant changes in the particle yields while changing the collected volume for group (ii) ($n = 5$, $p > 0.05$). Group (iii) provided ∼30 and ∼300 times lower yield than those of groups (ii) and (i), respectively (Figure 8c). In group (iii), we observed some statistical differences internally for different volumes of sample 1 ($n = 5$, $p < 0.01$) and sample 3 ($n = 5$, $p < 0.001$); but we did not observed the same behavior for sample 2 ($n = 5$, $p > 0.05$). In our experimental design, each sampling step was conducted after one refreshing step through the backwash process, and the same chip was used sequentially for all these sampling processes in a loop. Therefore, these fluctuations might be generated by the backwash steps, since the number of particles were lower in group (iii), and in particular, any effects caused by an earlier step would have larger impact on the yield of this group.

Likewise, through statistical assessments, we analyzed the data of backwash processes at different volumes of each experimental group (Figure 8d−f). In all cases regardless of the FBS condition, there was no difference between different volumes, pointing out that the refreshing performance was not hindered by the volume parameter ($n = 5$, $p > 0.05$). While evaluating the number of particles in Figure 8, the backwash steps of groups (i) and (ii) provided either similar or lower particles compared to their counterparts in the sample processes. However, the backwash steps of group (iii) were higher than their sample processes (Figure 8c,f), and this might be caused by the cake formation or the adherence of particles inside the microfluidic channel. As stated earlier, these two parameters would be more effective in terms of the yield since the number of exosome particles collected in group (iii) was lower than the other groups (i) and (ii), and any fluctuations in such parameters would interfere with the yield.

After analyzing through the NTA, the isolated exosome particles were imaged via the scanning electron microscope (Figure 9). Here, we evaluated the particles collected from FBS-free medium to minimize any interfering molecules in the FBS solution and observed that the isolated exosome particles were intact, and in some cases, there were some aggregated particles (Figure 9a). Moreover, we evaluated the particles on the filter membranes (upside of 200 nm filter and downside of 50 nm filter) to understand the cake formation (Figures 9b,c). The upside of the 200 nm filter had a lower number of particles, whereas we observed a higher number of particles downside of the 50 nm filter, pointing out a possible cake formation.

CONCLUSION

Among the extracellular particle isolation techniques, differential centrifugation is considered as the gold standard method; yet,

https://doi.org/10.1021/acs.langmuir.1c03119
Langmuir 2022, 38, 1897−1909

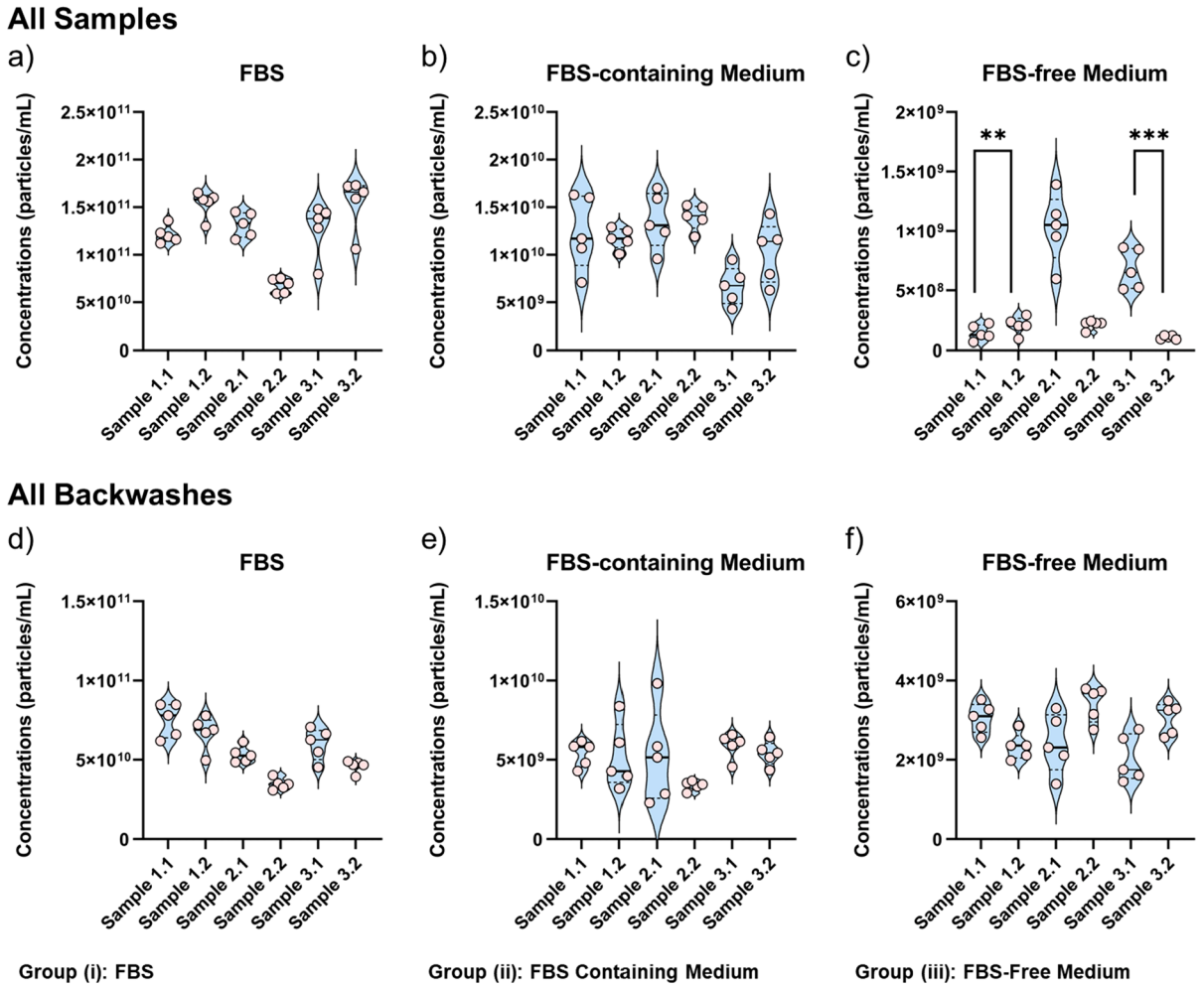

Figure 8. Evaluating all the groups and their particle yields. Samples of (a) group (i), (b) group (ii), and (c) group (iii) are examined for multiple use. Similarly, the backwashes of (d) group (i), (e) group (ii), and (f) group (iii) are examined for the purpose of multiple use. In the analysis, the particle concentrations of each group are evaluated individually. Statistical assessments are carried out using Violin-shaped Box–Whisker plots, and the data is further evaluated through nonparametric Kruskal–Wallis analysis followed by Dunn's multiple comparison test ($n = 5$; **: $p < 0.01$; ***: $p < 0.001$).

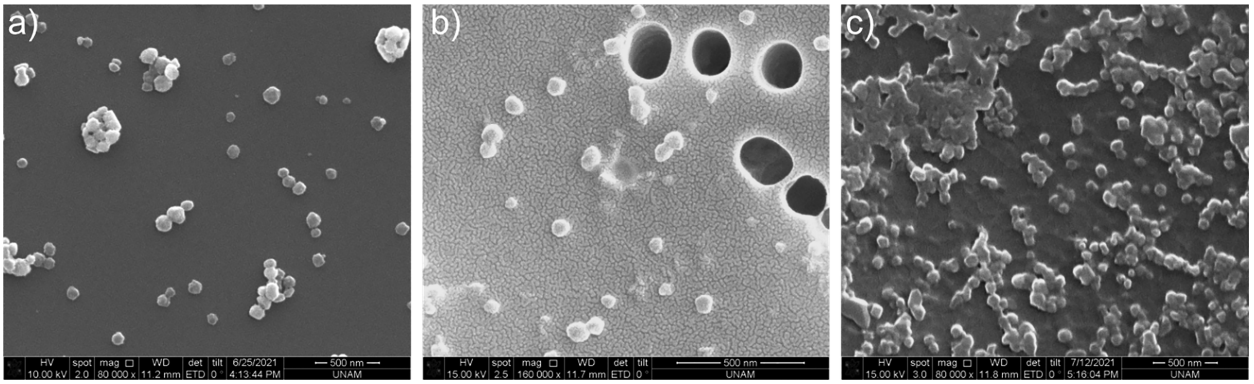

Figure 9. SEM images. (a) Isolated particles from group (iii). (b) Upside of the 200 nm filter is demonstrated where the supernatant is introduced. (c) Bottom side of the 50 nm filter shows potential cake formation.

this process impedes with (i) the loss of a considerable number of particles, thereby requiring a large volume of the initial sample; (ii) possible contamination of cell debris and other particles such as apoptotic bodies due to the consecutive centrifugation steps; and (iii) a lengthy assay time, user-dependent fashion, multistep procedure, and high-cost that would significantly impede its deployment and standardization.[39−45] Ultracentrifugation, mostly the density gradient version, is a modified version of a differential centrifugation method, which isolates particles through a density gradient. However, only a small volume of samples can be processed with this method, and contamination would notably interfere with their efficiency.[26,46] Size-exclusion chromatography usually impedes with prolonged assay time, limited sample volume,

https://doi.org/10.1021/acs.langmuir.1c03119
Langmuir 2022, 38, 1897−1909

and the contamination of similar size particles.[47] Although precipitation-based strategies utilizing polymeric substances hold significant impact in the field, interfering participation agents, molecular assembly/membrane fusion of particles, and coprecipitation of the other particles are still obstacles for this method.[48,49] On the other hand, immunoaffinity-based alternatives result in low-yield; highly rely on the antibody quality; and require other integrative systems such as sensor platforms or sophisticated cell counters, hence increasing their cost and hindering their utility in broader applications.[43,50−55]

Here, we have demonstrated a filter-integrated microfluidic platform that presents both dead-end and cross-flow approaches on the same device, thereby resulting in high-recovery and low clogging. For this manner, we comprehensively assessed the performance of microfluidic chips by changing (1) the medium condition and (2) volume parameter. We observed that FBS contains a rich source of readily and intrinsically accessible extracellular vesicles including particles with similar sizes like exosomes that would be included while benchmarking a newly introduced platform for particle isolation, especially for extracting exosome particles. Mostly, in the current design, the yield for isolating the particles was independent from the volume (1 or 2 mL). However, when having a low number of particles such as the ones isolated in the group (iii), any manipulation steps (sampling and backwashing) and volume would have an impact on the yield. In addition, we evaluated the repeatability of these chips through multiple sequential sampling and backwashing steps, and these chips completed all benchmarking steps successfully.

In addition, we here utilized two filter membranes with different pore sizes. Briefly, we first isolated larger particles on the first membrane (200 nm of pore diameter), and these particles traveled through the microchannels to reach the second membrane with smaller pore size (50 nm of pore diameter), where smaller particles were collected. On the basis of these pore diameters, we achieved the selective filtration at different sections (after the first and second membranes) of the chip. By only changing the pore diameters, different sizes of particles would be isolated, and the integration procedure for new filter membranes would be the same with our current protocol. For fine-tuning the particle sizes at different locations of the platform, a number of microfluidic chips would be connected serially through the tubings, thereby potentially minimizing any handling challenges, and also, enabling the processing of larger volumes at the same time. On the other hand, the flow rate parameter should be evaluated, especially for the filter membranes having smaller pores, in order to minimize any potential damages on the membrane structure.

In this study, we run the microfluidic platform for a single cell line. Moreover, this platform could be reused many times (at least three times as demonstrated in this study) for the same culture sample. While running the same sample solution having complex biological characteristics, there would be some protein aggregations that would clog the membrane pores, thereby potentially challenging the refreshing process. Since we here examined the FBS medium to mimic complex biomatrices, the current platform along with the defined procedure would achieve successful isolation of exosome particles with three times of reuse. Considering to increase the reuse numbers, the filter membranes would be modified with antifouling coating/materials, minimizing the nonspecific binding of proteins and cell debris,[56−59] and hence, the performance of the platform would be sustained for a longer term and higher number of reuses.

Moreover, while working with different matrices such as whole blood, removing cells would be performed by a simple centrifugation step,[60,61] thereby obtaining serum to run into the platform. This is a standardized cell separation and serum handling procedure that would not alter the current workflow significantly. While running different sample solutions from distinct cell types, potential cross-contamination risks need to be considered. For such experiments, the chip would be washed properly to refresh the filter membranes, thereby removing any possible debris or contaminants from the platform that would potentially interfere with the results of new sample solutions. As demonstrated, refreshing the membranes helped maximize the processed volume and allowed the same sample solution to be reused multiple times. Although we did not face any difficulties on the membranes on the course of sampling and refreshing, changing the flow rates (other than the ones stated in this study) would affect the membrane structure and robustness. For instance, higher flow rates would increase pressure drop on the membrane, leading to some damages that would potentially affect the platform performance for further experiments, as well as decreasing the quality of the permeate.

AUTHOR INFORMATION

Corresponding Author

Fatih Inci − *UNAM − National Nanotechnology Research Center, Bilkent University, 06800 Ankara, Turkey; Institute of Materials Science and Nanotechnology, Bilkent University, 06800 Ankara, Turkey;* orcid.org/0000-0002-9918-5038; Email: finci@bilkent.edu.tr

Complete contact information is available at: https://pubs.acs.org/10.1021/acs.langmuir.1c03119

Notes

The author declares no competing financial interest.

ACKNOWLEDGMENTS

Dr. Fatih Inci gratefully acknowledges the support from TÜBİTAK 2232-International Fellowship for Outstanding Researchers (Project 118C254) and Turkish Academy of Sciences-Outstanding Young Scientists Award Program (TÜBA-GEBİP). This publication has been produced benefiting from the 2232 International Fellowship for Outstanding Researchers Program of TÜBİTAK (Project 118C254). However, the entire responsibility of the publication/paper belongs to the owner of the publication/paper. The financial support received from TÜBİTAK does not mean that the content of the publication is approved in a scientific sense by TÜBİTAK. This work was supported by the BAGEP Award of the Science Academy. Dr. Inci also acknowledges the helpful discussions with Esma Derin, Eylul Gulsen Yildiz, and Saeedreza Zeibi Shirejini.

REFERENCES

(1) Singh, R. Chapter 1: Introduction to Membrane Technology. In *Membrane Technology and Engineering for Water Purification (Second ed.)*; Singh, R., Ed.; Butterworth-Heinemann: Waltham, MA, United States, 2015; pp 1−80, DOI: 10.1016/b978-0-444-63362-0.00001-x.

(2) Rackley, S. A. Chapter 8: Membrane Separation Systems. In *Carbon Capture and Storage (Second ed.)*; Rackley, S. A., Ed.; Butterworth-Heinemann: Cambridge, MA, United States, 2017; pp 187−225, DOI: 10.1016/b978-0-12-812041-5.00008-8.

(3) Luis, P. *Fundamental Modelling of Membrane Systems*; Luis, P., Ed.; Elsevier: Cambridge, MA, United States, 2018, DOI: 10.1016/c2016-0-02489-0.
(4) Glorieux, G.; Hulko, M.; Speidel, R.; Brodbeck, K.; Krause, B.; Vanholder, R. Looking beyond Endotoxin: A Comparative Study of Pyrogen Retention by Ultrafilters Used for the Preparation of Sterile Dialysis Fluid. *Sci. Rep.* **2015**, *4*, 6390.
(5) Koteshwara, A.; Philip, N. V.; Aranjani, J. M.; Hariharapura, R. C.; Volety Mallikarjuna, S. A Set of Simple Methods for Detection and Extraction of Laminarinase. *Sci. Rep.* **2021**, *11*, 2489.
(6) Miron, S. M.; Dutournié, P.; Thabet, K.; Ponche, A. Filtration of Protein-Based Solutions with Ceramic Ultrafiltration Membrane. Study of Selectivity, Adsorption, and Protein Denaturation. *C. R. Chim.* **2019**, *22* (2−3), 198−205.
(7) Palika, A.; Armanious, A.; Rahimi, A.; Medaglia, C.; Gasbarri, M.; Handschin, S.; Rossi, A.; Pohl, M. O.; Busnadiego, I.; Gübeli, C.; Anjanappa, R. B.; Bolisetty, S.; Peydayesh, M.; Stertz, S.; Hale, B. G.; Tapparel, C.; Stellacci, F.; Mezzenga, R. An Antiviral Trap Made of Protein Nanofibrils and Iron Oxyhydroxide Nanoparticles. *Nat. Nanotechnol.* **2021**, *16*, 918−925.
(8) Yang, D.; Zhang, W.; Zhang, H.; Zhang, F.; Chen, L.; Ma, L.; Larcher, L. M.; Chen, S.; Liu, N.; Zhao, Q.; Tran, P. H. L.; Chen, C.; Veedu, R. N.; Wang, T. Progress, Opportunity, and Perspective on Exosome Isolation - Efforts for Efficient Exosome-Based Theranostics. *Theranostics* **2020**, *10* (8), 3684−3707.
(9) Wang, S. Q.; Sarenac, D.; Chen, M. H.; Huang, S. H.; Giguel, F. F.; Kuritzkes, D. R.; Demirci, U. Simple Filter Microchip for Rapid Separation of Plasma and Viruses from Whole Blood. *Int. J. Nanomedicine* **2012**, *7*, 5019−5028.
(10) Inan, H.; Wang, S.; Inci, F.; Baday, M.; Zangar, R.; Kesiraju, S.; Anderson, K. S.; Cunningham, B. T.; Demirci, U. Isolation, Detection, and Quantification of Cancer Biomarkers in HPV-Associated Malignancies. *Sci. Rep.* **2017**, *7* (1), 3322.
(11) Saylan, Y.; Erdem, Ö.; Ünal, S.; Denizli, A. An Alternative Medical Diagnosis Method: Biosensors for Virus Detection. *Biosensors* **2019**, *9*, 65.
(12) Paulaitis, M.; Agarwal, K.; Nana-Sinkam, P. Dynamic Scaling of Exosome Sizes. *Langmuir* **2018**, *34* (32), 9387−9393.
(13) Karpman, D.; Ståhl, A.-L.; Arvidsson, I. Extracellular Vesicles in Renal Disease. *Nat. Rev. Nephrol.* **2017**, *13* (9), 545−562.
(14) Shao, H.; Im, H.; Castro, C. M.; Breakefield, X.; Weissleder, R.; Lee, H. New Technologies for Analysis of Extracellular Vesicles. *Chem. Rev.* **2018**, *118* (4), 1917−1950.
(15) Xiao, X.; Wang, J.; Liu, Y.; Fan, R.; Liu, L.; Ma, X.; Bi, K.; Chen, Y.; Zhao, B.; Bihl, J. Cellular Membrane Microparticles: Potential Targets of Combinational Therapy for Vascular Disease. *Curr. Vasc. Pharmacol.* **2015**, *13* (4), 449−458.
(16) Burger, D.; Schock, S.; Thompson, C. S.; Montezano, A. C.; Hakim, A. M.; Touyz, R. M. Microparticles: Biomarkers and Beyond. *Clin. Sci.* **2013**, *124* (7), 423−441.
(17) Kourembanas, S. Exosomes: Vehicles of Intercellular Signaling, Biomarkers, and Vectors of Cell Therapy. *Annu. Rev. Physiol.* **2015**, *77* (1), 13−27.
(18) Barteneva, N. S.; Fasler-Kan, E.; Bernimoulin, M.; Stern, J. N. H.; Ponomarev, E. D.; Duckett, L.; Vorobjev, I. A. Circulating Microparticles: Square the Circle. *BMC Cell Biol.* **2013**, *14*, 23.
(19) Ferruzzi, P.; Zocco, D.; Cappello, F.; Kuo, W. P.; Fais, S. Extracellular Vesicles as Shuttles of Tumor Biomarkers and Anti-Tumor Drugs. *Front. Oncol.* **2014**, *4*, 267.
(20) Mora, E. M.; Álvarez-Cubela, S.; Oltra, E. Biobanking of Exosomes in the Era of Precision Medicine: Are We There Yet. *Int. J. Mol. Sci.* **2016**, *17* (1), 13.
(21) Tao, S. C.; Guo, S. C.; Zhang, C. Q. Modularized Extracellular Vesicles: The Dawn of Prospective Personalized and Precision Medicine. *Adv. Sci.* **2018**, *5*, 1700449.
(22) Erdbrugger, U.; Le, T. H. Extracellular Vesicles in Renal Diseases: More than Novel Biomarkers? *J. Am. Soc. Nephrol.* **2016**, *27* (1), 12−26.
(23) Gould, S. J.; Raposo, G. As We Wait: Coping with an Imperfect Nomenclature for Extracellular Vesicles. *J. Extracell. Vesicles* **2013**, *2*, 20389.
(24) Colombo, M.; Raposo, G.; Théry, C. Biogenesis, Secretion, and Intercellular Interactions of Exosomes and Other Extracellular Vesicles. *Annu. Rev. Cell Dev. Biol.* **2014**, *30*, 255−289.
(25) Liangsupree, T.; Multia, E.; Riekkola, M. L. Modern Isolation and Separation Techniques for Extracellular Vesicles. *J. Chromatogr. A* **2021**, *1636*, 461773.
(26) Shirejini, S. Z.; Inci, F. The Yin and Yang of Exosome Isolation Methods: Conventional Practice, Microfluidics, and Commercial Kits. *Biotechnol. Adv.* **2022**, *54*, 107814.
(27) Lv, X.; Geng, Z.; Su, Y.; Fan, Z.; Wang, S.; Fang, W.; Chen, H. Label-Free Exosome Detection Based on a Low-Cost Plasmonic Biosensor Array Integrated with Microfluidics. *Langmuir* **2019**, *35* (30), 9816−9824.
(28) Lobb, R. J.; Becker, M.; Wen Wen, S.; Wong, C. S. F.; Wiegmans, A. P.; Leimgruber, A.; Möller, A. Optimized Exosome Isolation Protocol for Cell Culture Supernatant and Human Plasma. *J. Extracell. Vesicles* **2015**, *4* (1), 27031.
(29) Tauro, B. J.; Greening, D. W.; Mathias, R. A.; Ji, H.; Mathivanan, S.; Scott, A. M.; Simpson, R. J. Comparison of Ultracentrifugation, Density Gradient Separation, and Immunoaffinity Capture Methods for Isolating Human Colon Cancer Cell Line LIM1863-Derived Exosomes. *Methods* **2012**, *56* (2), 293−304.
(30) Thomas, P.; Smart, T. G. HEK293 Cell Line: A Vehicle for the Expression of Recombinant Proteins. *J. Pharmacol. Toxicol. Methods* **2005**, *51* (3), 187−200.
(31) Ben Salem, I.; Prola, A.; Boussabbeh, M.; Guilbert, A.; Bacha, H.; Abid-Essefi, S.; Lemaire, C. Crocin and Quercetin Protect HCT116 and HEK293 Cells from Zearalenone-Induced Apoptosis by Reducing Endoplasmic Reticulum Stress. *Cell Stress Chaperones* **2015**, *20* (6), 927−938.
(32) Lehrich, B. M.; Liang, Y.; Khosravi, P.; Federoff, H. J.; Fiandaca, M. S. Fetal Bovine Serum-Derived Extracellular Vesicles Persist within Vesicle-Depleted Culture Media. *Int. J. Mol. Sci.* **2018**, *19* (11), 3538.
(33) Angelini, F.; Ionta, V.; Rossi, F.; Miraldi, F.; Messina, E.; Giacomello, A. Foetal Bovine Serum-Derived Exosomes Affect Yield and Phenotype of Human Cardiac Progenitor Cell Culture. *BioImpacts* **2016**, *6* (1), 15−24.
(34) Sampson, R. A. On Stokes's Current Function. *Philos. Trans. R. Soc. A* **1891**, *182*, 449−518.
(35) Weissberg, H. L. End Correction for Slow Viscous Flow through Long Tubes. *Phys. Fluids* **1962**, *5* (9), 1033−1036.
(36) Dagan, Z.; Weinbaum, S.; Pfeffer, R. An Infinite-Series Solution for the Creeping Motion through an Orifice of Finite Length. *J. Fluid Mech.* **1982**, *115*, 505−523.
(37) Devireddy, L. R.; Myers, M.; Screven, R.; Liu, Z.; Boxer, L. A Serum-Free Medium Formulation Efficiently Supports Isolation and Propagation of Canine Adipose-Derived Mesenchymal Stem/Stromal Cells. *PLoS One* **2019**, *14* (2), e0210250.
(38) Zhu, Q.; Huang, Y.; Yang, Q.; Liu, F. Recent Technical Advances to Study Metabolomics of Extracellular Vesicles. *Microchem. J.* **2021**, *171*, 106816.
(39) Witwer, K. W.; Buzas, E. I.; Bemis, L. T.; Bora, A.; Lasser, C.; Lotvall, J.; Nolte-'t Hoen, E. N.; Piper, M. G.; Sivaraman, S.; Skog, J.; Thery, C.; Wauben, M. H.; Hochberg, F. Standardization of Sample Collection, Isolation and Analysis Methods in Extracellular Vesicle Research. *J. Extracell. vesicles* **2013**, *2*, 20360.
(40) Livshits, M. A.; Khomyakova, E.; Evtushenko, E. G.; Lazarev, V. N.; Kulemin, N. A.; Semina, S. E.; Generozov, E. V.; Govorun, V. M. Isolation of Exosomes by Differential Centrifugation: Theoretical Analysis of a Commonly Used Protocol. *Sci. Rep.* **2015**, *5*, 17319.
(41) Liang, L.-G.; Sheng, Y.-F.; Zhou, S.; Inci, F.; Li, L.; Demirci, U.; Wang, S. An Integrated Double-Filtration Microfluidic Device for Detection of Extracellular Vesicles from Urine for Bladder Cancer Diagnosis. *Methods Mol. Biol.* **2017**, *1660*, 355.
(42) Liang, K.; Liu, F.; Fan, J.; Sun, D.; Liu, C.; Lyon, C. J.; Bernard, D. W.; Li, Y.; Yokoi, K.; Katz, M. H.; Koay, E. J.; Zhao, Z.; Hu, Y.

Nanoplasmonic Quantification of Tumour-Derived Extracellular Vesicles in Plasma Microsamples for Diagnosis and Treatment Monitoring. *Nat. Biomed. Eng.* **2017**, *1* (4), 1−11.
(43) Liang, L. G.; Kong, M. Q.; Zhou, S.; Sheng, Y. F.; Wang, P.; Yu, T.; Inci, F.; Kuo, W. P.; Li, L. J.; Demirci, U.; Wang, S. Q. An Integrated Double-Filtration Microfluidic Device for Isolation, Enrichment and Quantification of Urinary Extracellular Vesicles for Detection of Bladder Cancer. *Sci. Rep.* **2017**, *7*, 46224.
(44) Merchant, M. L.; Rood, I. M.; Deegens, J. K. J.; Klein, J. B. Isolation and Characterization of Urinary Extracellular Vesicles: Implications for Biomarker Discovery. *Nat. Rev. Nephrol.* **2017**, *13* (12), 731−749.
(45) Taylor, D. D.; Shah, S. Methods of Isolating Extracellular Vesicles Impact Down-Stream Analyses of Their Cargoes. *Methods* **2015**, *87*, 3−10.
(46) Lane, R. E.; Korbie, D.; Anderson, W.; Vaidyanathan, R.; Trau, M. Analysis of Exosome Purification Methods Using a Model Liposome System and Tunable-Resistive Pulse Sensing. *Sci. Rep.* **2015**, *5*, 7639.
(47) Böing, A. N.; Van Der Pol, E.; Grootemaat, A. E.; Coumans, F. A. W.; Sturk, A.; Nieuwland, R. Single-Step Isolation of Extracellular Vesicles by Size-Exclusion Chromatography. *J. Extracell. vesicles* **2014**, *3* (1), 23430.
(48) Zarovni, N.; Corrado, A.; Guazzi, P.; Zocco, D.; Lari, E.; Radano, G.; Muhhina, J.; Fondelli, C.; Gavrilova, J.; Chiesi, A. Integrated Isolation and Quantitative Analysis of Exosome Shuttled Proteins and Nucleic Acids Using Immunocapture Approaches. *Methods* **2015**, *87*, 46−58.
(49) Posokhov, Y. O.; Kyrychenko, A. Effect of Acetone Accumulation on Structure and Dynamics of Lipid Membranes Studied by Molecular Dynamics Simulations. *Comput. Biol. Chem.* **2013**, *46*, 23−31.
(50) Poellmann, M. J.; Nair, A.; Bu, J.; Kim, J. K. H.; Kimple, R. J.; Hong, S. Immunoavidity-Based Capture of Tumor Exosomes Using Poly(Amidoamine) Dendrimer Surfaces. *Nano Lett.* **2020**, *20* (8), 5686−5692.
(51) Liu, Z.; Wang, H.; Li, J.; Wang, M.; Yang, H.; Si, F.; Kong, J. Detection of Exosomes via an Electrochemical Biosensor Based on C60-Au-Tb Composite. *Microchem. J.* **2021**, *170*, 106772.
(52) Inci, F.; Celik, U.; Turken, B.; Özer, H. Ö.; Kok, F. N. Construction of P-Glycoprotein Incorporated Tethered Lipid Bilayer Membranes. *Biochem. Biophys. Rep.* **2015**, *2*, 115−122.
(53) Erdem, Ö.; Eş, I.; Akceoglu, G. A.; Saylan, Y.; Inci, F. Recent Advances in Microneedle-Based Sensors for Sampling, Diagnosis and Monitoring of Chronic Diseases. *Biosensors* **2021**, *11* (9), 296.
(54) Inci, F.; Saylan, Y.; Kojouri, A. M.; Ogut, M. G.; Denizli, A.; Demirci, U. A Disposable Microfluidic-Integrated Hand-Held Plasmonic Platform for Protein Detection. *Appl. Mater. Today* **2020**, *18*, 100478.
(55) Erdem, Ö.; Derin, E.; Zeibi Shirejini, S.; Sagdic, K.; Yilmaz, E. G.; Yildiz, S.; Akceoglu, G. A.; Inci, F. Carbon-Based Nanomaterials and Sensing Tools for Wearable Health Monitoring Devices. *Adv. Mater. Technol.* **2021**, 2100572.
(56) Inci, F.; Ozen, M. O.; Saylan, Y.; Miansari, M.; Cimen, D.; Dhara, R.; Chinnasamy, T.; Yuksekkaya, M.; Filippini, C.; Kumar, D. K.; Calamak, S.; Yesil, Y.; Durmus, N. G.; Duncan, G.; Klevan, L.; Demirci, U. A Novel On-Chip Method for Differential Extraction of Sperm in Forensic Cases. *Adv. Sci.* **2018**, *5*, 1800121.
(57) Saylan, Y.; Erdem, Ö.; Inci, F.; Denizli, A. Advances in Biomimetic Systems for Molecular Recognition and Biosensing. *Biomimetics* **2020**, *5* (2), 20.
(58) Inci, F.; Karaaslan, M. G.; Gupta, R.; Avadhani, A.; Ogut, M. G.; Atila, E. E.; Duncan, G.; Klevan, L.; Demirci, U. BIO-INSPIRED MAGNETIC BEADS FOR ISOLATION OF SPERM FROM HETEROGENOUS SAMPLES IN FORENSIC APPLICATIONS. *Forensic Sci. Int. Genet.* **2021**, *52*, 102451.
(59) Akceoglu, G. A.; Saylan, Y.; Inci, F. A Snapshot of Microfluidics in Point-of-Care Diagnostics: Multifaceted Integrity with Materials and Sensors. *Adv. Mater. Technol.* **2021**, *6*, 2100049.
(60) Mani, V.; Paleja, B.; Larbi, K.; Kumar, P.; Tay, J. A.; Siew, J. Y.; Inci, F.; Wang, S. Q.; Chee, C.; Wang, Y. T.; Demirci, U.; De Libero, G.; Singhal, A. Microchip-Based Ultrafast Serodiagnostic Assay for Tuberculosis. *Sci. Rep.* **2016**, *6* (1), 35845.
(61) Wang, K.; Seol, H.; Liu, X.; Wang, H.; Cheng, G.; Kim, S. Ultralow-Fouling Zwitterionic Polyurethane-Modified Membranes for Rapid Separation of Plasma from Whole Blood. *Langmuir* **2021**, *37* (33), 10115−10125.

https://doi.org/10.1021/acs.langmuir.1c03119
Langmuir 2022, 38, 1897−1909